RSC Advances

This article can be cited before page numbers have been issued, to do this please use: Y. Patil, R. Misra, M. L. Keshtov, F. Chen and G. D. Sharma, *RSC Adv.*, 2016, DOI: 10.1039/C6RA10442H.

ROYAL SOCIETY OF CHEMISTRY

www.rsc.org/advances

View Article Online
DOI: 10.1039/C6RA10442H

Symmetrical and Unsymmetrical Triphenylamine based Diketopyrrolopyrroles and their use as Donor for Solution Processed Bulk Heterojunction Organic Solar Cells

Yuvraj Patil[a], Rajneesh Misra*[a], F. C. Chen[b], M. L. Keshtov[c], Ganesh D. Sharma[d]*

[a]Department of Chemistry
Indian Institute of Technology, Indore (MP) 453552, India
[b]Department of Photonics, National Chiao Tung University, 1001 University Road, Hsinchu 30010, Taiwan
[c]A. N. Nesmeyanov Institute of Organoelement Compounds, Russian Academy of Sciences, Vavilova Str., 28, Moscow 119991, Russia
[d]Department of Physics, The LNM Institute of Information Technology, Jamdoli, Jaipur, 303031, India

Abstract

Two small molecules **DPP3** (D-π-A) and **DPP4** (D-π-A-π-D) with triphenylamine (TPA) donor and diketopyrrolopyrrole (DPP) acceptor linked with ethyne linker were designed and synthesized by the Pd-catalyzed Sonogashira cross-coupling reaction. Their photonic, electronic, thermal and computational properties were investigated. The red shift in the electronic absorption spectra of **DPP4** as compared to **DPP3** is related to extended conjugation and increased donor-acceptor interaction. We have used **DPP3** and **DPP4** as electron donor along with $PC_{71}BM$ as electron acceptor for the solution processed bulk heterojunction organic solar cells. The solar cells prepared from **DPP3**:$PC_{71}BM$ and **DPP4**:$PC_{71}BM$ (1:2) processed from chloroform (CF) exhibit a power conversion efficiency (PCE) of 2.23% (J_{sc} = 6.74 mA/cm^2, V_{oc}= 0.92V and FF = 036) and 3.05% (J_{sc} = 8.26 mA/cm^2, V_{oc} = 0.88 V and FF = 0.42), respectively. The higher PCE of the device with **DPP4** compared to **DPP3** was demonstrated to the higher hole mobility and broader IPCE spectra. The devices based on **DPP3**:$PC_{71}BM$ and **DPP4**:$PC_{71}BM$ processed with solvent additive (1v% DIO, 1, 8-diiodooctane) showed PCE of 4.06% and 5.31%, respectively. The device optimization results from the improvement of the balanced charge transport and better nanoscale morphology induced by the solvent additive.

Keywords: Diketopyrrolopyrrole, Bulk heterojunction, Organic Solar Cells, Power Conversion Efficiency, Solvent Additives

*Corresponding authors E-mail: rajneeshmisra@iiti.ac.in (Rajneesh Misra), gdsharma273@gmail.com (Ganesh D Sharma)

View Article Online
DOI: 10.1039/C6RA10442H

Introduction

Bulk heterojunction (BHJ) solar cell from a blend of electron donor and electron acceptor organic semiconducting materials are potential source of renewable energy sources due to being inexpensive and lightweight with flexibility. [1] The research on the organic solar cell (OSC) materials have been currently being focused on the design and synthesis of low bandgap conjugated polymers that are capable of both light absorption and charge transport. After the optimization of bandgap and electrochemical energy levels of conjugated polymer donors, control of nanomorphology of the BHJ active layer, and interfacial layers, the power conversion efficiency (PCE) of OSCs based on these materials has exceed 10%.[2] In spite of this advancement, these materials suffer from several drawbacks, such as batch to batch variation, side length polydispersity, structural defects and difficult synthesis and purification. [3] To overcome these limitations the research is diverted to "small molecule" BHJ (SM-BHJ) solar cells, where polymer donors were replaced by the conjugated molecular systems which can be synthesized with well defined molecular architecture with desired frontier molecular orbitals to match the light harvesting of the best performing polymeric materials. [4] The PCE of SM-BHJs has been reached in the range of 9-10%. [5] The PCE of SM-BHJ solar cells could be further improved by exploring the design of new SMs that can used as donor in BHJ active layer.

The frequently used strategy to design high performance organic small molecule is to use the push-pull chromophore structure in which electron donating (D) and electron accepting (A) units are coupled together, designing semiconducting organic materials with highly conjugated backbone structure. [6] This type of small molecules exhibit low band gap, intense absorption in visible region, strong intra- and intermolecular interaction, and efficient charge transport, which is beneficial for high PCE of organic solar cells. Among the various SMs, designed for OSCs, the SMs containing diketopyrrolopyrrole (DPP), with two fused electron deficient lactam rings have been attracted lot of attention because of its unique properties such as high absorption coefficient in visible region, strong electron withdrawing property and high coplanarity facilitate intermolecular packing. DPP derivatives possess high thermal stability and used as brilliant colorants. [7] The DPP is reported as potential electron acceptor and functionalization with electron donor will results in donor-acceptor molecular system. Moreover, strong donor –acceptor (D-A) interaction between DPP core and adjacent thiophenes generate strongly hybridized frontier molecular orbitals, low lying LUMO and high lying HOMO orbitals of DPP based SMs. Therefore, most of the SMs with DPP

View Article Online
DOI: 10.1039/C6RA10442H

possesses low band gap and well ordered structure in thin film and thus exhibit high J_{sc} in OSCs. [8, 11] The state of art with the PCE of 7% has been reported for BHJ solar cells based on DPP SMs [9] and in the range of 6 – 9% for DPP based D–A copolymers. [10] Our group is involved in the design and synthesis of donor–acceptor molecular systems with low HOMO–LUMO gap for optoelectronic applications. [11] Ziessel *et. al*. have reported the symmetrical and unsymmetrical triphenylamine functionalized diketopyrrolopyrroles. [12]

In this article we wish to report the synthesis and solar cell properties of **DPP3** and **DPP4** as electron donor along with $PC_{71}BM$ as electron acceptor in solution processed BHJ organic solar cells. The acetylene linker between DPP and TPA is used to afford the low HOMO-LUMO gap through extended conjugation and also increase the ionization potential of resulting molecule due to relatively larger electron-withdrawing characteristics of sp hybridization over sp^2 hybridization. [13] After the optimization, we have achieved the PCE of 4.06% and 5.31% for active layer **DPP3**:$PC_{71}BM$ and **DPP4**:$PC_{71}BM$, respectively.

Experimental part

Synthesis of DPP3

In 100 ml round bottom flask monobromodiketopyrrolopyrrole **1** (0.100 g, 0.15 mmol) and (4-ethynylphenyl) diphenylamine (0.041 g, 0.15 mmol) were dissolved in dry THF (10 ml) and triethylamine (6 ml). The reaction mixture was degassed with argon for 10 minutes and $Pd(PPh_3)_4$ (0.0.018 g, 0.015 mmol) and CuI (0.0028 g, 0.015 mmol) were added. The reaction mixture was stirred at 70 ^oC for 24 hours. After completion of reaction, the reaction mixture was allowed to cool down to room temperature. The solvents were removed under vacuo and the product was purified by silica-column chromatography with hexane: dichloromethane (3:1) as an eluent in 75% yield.

^1H NMR (400 MHz, $CDCl_3$, δ in ppm): 8.93 (2H, s), 7.64 (1H, s), 7.36 (3H, m), 7.28 (4H, m), 7.12 (7H, m), 7.00 (2H, d, J = 8 Hz), 4.05 (4H, s), 2.35 (1H, s), 1.74 (4H, s), 1.41 (4H, s), 1.25 (23 H, s), 0.86 (6H, s); ^{13}C NMR (100 MHz, $CDCl_3$, δ in ppm): 161.3, 161.2, 148.7, 146.9, 139.9, 139.1, 135.5, 135.4, 132.6, 132.5, 130.8, 129.9, 129.8, 129.5, 129.2, 128.7, 125.3, 124.0, 121.6, 114.5, 108.3, 107.9, 98.5, 81.7, 42.3, 31.9, 30.1, 30.0, 29.5, 29.31, 29.26, 26.9, 22.7, 14.1; HRMS (ESI) *m/z* calcd for $C_{54}H_{61}N_3O_2S_2$ + Na: 870.4097 $[M + Na]^+$, found 870.4094 $[M + Na]^+$.

Synthesis of DPP4

In 100 ml round bottom flask dibromodiketopyrrolopyrrole **2** (0.100 g, 0.14 mmol) and (4-ethynylphenyl) diphenylamine (0.073 g, 0.28 mmol) were dissolved in dry THF (10 ml) and

View Article Online
DOI: 10.1039/C6RA10442H

triethylamine (6 ml). The reaction mixture was degassed with argon for 10 minutes and $Pd(PPh_3)_4$ (0.015 g, 0.014 mmol) and CuI (0.0025 g, 0.014 mmol) were then added. The reaction mixture was stirred at 70 ^oC for 24 hours. After completion, the reaction mixture was allowed to cool down to room temperature. The solvents were removed under vacuo and colored product was purified by silica-column chromatography with hexane: dichloromethane (3:1) as an eluent in 80% yield.

^1H NMR (400 MHz, $CDCl_3$, δ in ppm): 8.93 (2H, s), 7.36 (6H, m), 7.29 (9H, m), 7.10 (11H, m), 7.00 (4H, d, J = 8 Hz), 4.07 (4H, m), 3.13 (2H, m), 1.75 (4H, m), 1.45 (6H, m), 1.25 (21H, s), 0.85 (6H, m); ^{13}C NMR (100 MHz, $CDCl_3$, δ in ppm): 161.2, 148.7, 147.0, 139.0, 135.7, 132.6, 130.0, 129.7, 129.5, 129.4, 125.4, 124.0, 121.7, 114.5, 108.5, 98.7, 81.8, 46.1, 42.4, 31.9, 30.1, 29.7, 29.6, 29.31, 29.26, 26.9, 22.7, 14.2, 8.7; HRMS (ESI) *m/z* calcd for $C_{74}H_{74}N_4O_2S_2$ + Na: 1137.5145 $[M + Na]^+$, found 1137.5127 $[M + Na]^+$.

Results and discussion

The small molecules **DPP3** and **DPP4** were synthesized by Pd-catalyzed Sonogashira cross-coupling reaction of mono-bromo DPP **1** and di-bromo DPP **2** with one and two equivalents of (4-ethynylphenyl) diphenylamine in 75% and 80% yield respectively (Scheme 1). The precursors mono-bromo DPP **1** and di-bromo DPP **2** were synthesized by following reported procedure. [14] The **DPP3** and **DPP4** were purified by repeated silica-gel column chromatography and recrystallization techniques. Both the DPPs are readily soluble in common organic solvents like dichloromethane, chloroform, toluene, tetrahydrofuran and were well characterized by ^1H NMR, ^{13}C NMR, and HRMS techniques.

Photophysical and Thermal Properties

The electronic absorption spectra of **DPP3** and **DPP4** in dilute chloroform (CF) solution as well thin film cast from CF, are shown in Fig. 1 and data are listed in Table 1. Both the DPPs show absorption bands in UV-Visible region from 300 nm to 750 nm. The absorption bands at shorter (below 500 nm) and longer wavelength (510-750 nm) correspond to the π–π* transition and intramolecular charge transfer (ICT) from TPA to DPP respectively. The red shift of CT band in **DPP4** as compared to **DPP3** is related to the extended conjugation and increased donor-acceptor interaction. The more intense absorption for **DPP4** may be due to the presence of two TPA fragments is likely to be attributed to an internal charge transfer induced by the strongly electron donating TPA unit and the π-accepting DPP unit. Moreover, both materials have shown vibrational absorption peaks in the

View Article Online
DOI: 10.1039/C6RA10442H

higher wavelength region. In contrast, the absorption spectra of these DPP SMs in thin films are red shifted compared to those in solution. Such feature is attributed to a more planar conjugated backbone, further ordered structure in solid state and a higher π-electron delocalization though the molecular backbone, which could be beneficial to greater hole mobility. The optical bandgaps of these **DPP3** and **DPP4** were estimated from the onset edge of absorption spectra in thin film and are 1.84 and 1.72 eV, respectively.

The thermal properties of **DPP3** and **DPP4** were investigated by thermogravimetric analysis (TGA) under nitrogen atmosphere and curves shown in Fig. S1. The decomposition temperatures for 10% weight loss in **DPP3** and **DPP4** were 402 °C and 398 °C, respectively (Table 1), indicating that both DPPs are more thermally stable.

Electrochemical and Computational Properties

The electrochemical properties of DPPs were explored by cyclic voltammetry and differential pulse voltammetry (CV and DPV) techniques in dichloromethane solvent using 0.1 M tetrabutylammonium hexafluorophosphate (Bu_4NPF_6) as supporting electrolyte. The CV and are shown in Fig. 2 and the corresponding data are listed in Table 2. Both the DPPs exhibit four oxidation waves. The first oxidation potential of **DPP3** and **DPP4** are almost same. The **DPP3** and **DPP4** show two reduction waves in CV and DPV corresponding to formation of mono and dianion. The potentials were measured vs Ag/Ag^+ as quasi reference electrode. After each experiment, the potential of the Ag/Ag^+ electrode was calibrated against the Fc/Fc^+ redox couple.

The HOMO and LUMO energy levels were estimated from the onset oxidation and reduction potentials respectively. The HOMO/LUMO energy levels are -5.12/-3.69 eV and -5.07/-3.77 eV for **DPP3** and **DPP4**, respectively. Because the exciton binding energy in an organic semiconductor is 0.3 – 0.5 eV, the LUMO offset between **DPP3** or **DPP4** and $PC_{71}BM$ afford sufficient driving force for efficient exciton dissociation and effective electron transfer in the active layer. The deeper HOMO energy level is desirable to achieve the high V_{oc}, since V_{oc} is determined by the energy difference between the HOMO level of donor and LUMO energy of acceptor used in the active layer of BHJ organic solar cell.

The density functional theory (DFT) calculations were carried to understand the geometry and electronic structure of **DPP3** and **DPP4** using the Gaussian09W program at the B3LYP/6-31+G** level**.** The geometry optimizations were carried out in the gas phase and frontier molecular orbitals (FMOs) are displayed in Fig. 3. The HOMO of both the DPPs are

View Article Online
DOI: 10.1039/C6RA10442H

distributed on the whole molecule whereas LUMOs are localized mainly on the DPP core. The localization of LUMO on DPP core indicates the acceptor nature of DPP**.** This shows the typical donor–acceptor (D–A) interaction and charge transfer from TPA to DPP. [15] The theoretical band gap values obtained from DFT calculations were found to be in consistent with the electrochemical band gap values calculated from DPV and the optical band gap values from the UV-vis absorption (Table 1).

Photovoltaic properties

The solution processed BHJ solar cells based on **DPP3** and **DPP4** as donor along with $PC_{71}BM$ as acceptor were made with a device structure ITO/PEDOT:PSS/**DPP3** or **DPP4**:$PC_{71}BM$/ Al. The **DPP3** or **DPP4**:$PC_{71}BM$ active layer was formed by spin coating of a constant concentration of 14 mg/mL, compromising a mixture of **DPP3** or **DPP4** and $PC_{71}BM$ in CF. The photovoltaic performance of the BHJ organic solar cells are strongly influenced by the concentration of donor and acceptor component used in the active layer, since there should be a balance between the absorption profile of active layer and charge transport within the active layer towards the final collecting electrodes. The weight ratio between **DPP**s and $PC_{71}BM$ were varied from 1:1, 1:1.5, 1:2 and 1:2.5 in order to optimize the ratio of donor and acceptor in active layer. The best performance was achieved for the 1:2 weight ratio for both the DPPs as donor. We have observed that the higher concentration of donor reduced the electron mobility leading the reduction of PCE, may be attributed to the poor interpenetrating pathways between the donor and acceptor. Furthermore, the concentration of DIO solvent additive was varied from 0 to 0.5%, 1% and 1.5% in order to improve the morphology of BHJ active layer. It was observed that the optimized weight ratio is 1:2 and solvent concentration is 1% of DIO in CF solution. The current–voltage (J-V) characteristics of the optimized devices based on **DPP3**:$PC_{71}BM$ and **DPP4**:$PC_{71}BM$ active layers cast from CF solution are shown in Fig. 4a and 4c, respectively and photovoltaic parameters are summarized in Table 3. Under optimized **DPP3**:$PC_{71}BM$ (1:2) cast from CF based device showed relatively high V_{oc} of 0.92 V, but low PCE of 2.23% with a J_{sc} of 6.74 mA/cm^2 and FF of 0.36. However, under the similar condition, the device based on **DPP4**:$PC_{71}BM$ exhibited a PCE of 3.05% with J_{sc} of 8.26 mA/cm^2, V_{oc} of 0.88 V and FF of 0.42. The increase in PCE for the **DPP4** based device is mainly due to the higher values of J_{sc} and FF. The relatively higher V_{oc} for **DPP3** based device is proportional to its slightly deeper HOMO energy level compared to **DPP4**. The higher value of J_{sc} for **DPP4** is also confirmed from the IPCE spectra of the devices (Fig. 4b and 4d). The IPCE spectra of devices based on

View Article Online
DOI: 10.1039/C6RA10442H

DPP3 and **DPP4** exhibited broad response, consistent with absorption spectra of their corresponding active layers (Fig. 4a and 4b). It can be seen from the Fig. that absorption spectra of the **DPP**s:$PC_{71}BM$ blends is the combination of both $PC_{71}BM$ and DPPs (the absorption band corresponds around 390 nm, attributed to $PC_{71}BM$ whereas the absorption band in longer wavelength region corresponds to DPPs), indicating both $PC_{71}BM$ and DPP are contributing to the exciton generation and resulting photocurrent in the device. Comparing the Fig. 3b and 3d, it can be seen that **DPP3** based device showed response from 350 – 660 nm with maximum IPCE value of 31% at 610 nm, whereas **DPP4** based device showed IPCE response from 350 to 690 nm with maximum value of 40% at 624 nm. The J_{sc} values of **DPP3** and **DPP4** based devices calculated from the integration of IPCE spectra are 6.58 mA/cm^2 and 8.14 mA/cm^2, respectively, which are consistent with the measured values from J-V characteristics under illumination.

We measured the J-V characteristics of hole only devices based on **DPP3**:$PC_{71}BM$ and **DPP4**:$PC_{71}BM$ (weight ratio 1:2) active layers (as shown in Figure 5a and 5b), and applied space charge limited current (SCLC) model to extract hole mobility (μ_h) using hole only device configuration ITO/PEDOT:PSS/ active layer/Au. The estimated values of hole mobility for **DPP3** and **DPP4** are 5.34 x10^{-6} and 7.82 x10^{-6} cm^2/Vs, respectively (Table 3). Moreover, we have also estimated the electron mobilities (μ_e) in the active layers using similar manner employing electron only device (ITO/Al/active layer/Al), are 2.34 x 10^{-4} cm^2/Vs and 2.42 x10^{-4} cm^2 for **DPP3** and **DPP4** based active layer. This indicates that the electron to hole mobility ratio for **DPP3** and **DPP4** based devices is 44 and 31, respectively. Although in both devices, the electron and hole transport in unbalanced resulting lower PCE, but relatively more balanced charge transport for **DPP4** based device, leading to relatively higher PCE for this device as compared to **DPP3** based device.

The PCE of the devices processed with CF solution is moderate. Although the V_{oc} is quite respectable but the low value of PCE is mainly due to the low J_{sc} and FF. It is well known that the high J_{sc} of the BHJ organic solar cell is related to the exciton generation and dissociation at D-A interface and their efficient charge transport with any recombination losses during their transportation towards the electrodes and directly linked with the nanophase morphology of the BHJ active layer. The nanomorphology of the BHJ active layer can be strongly affected by the processing conditions. [16] A small amount of DIO was employed as solvent additive to improve the nanophase morphology of the active layer to improve the exciton diffusion and dissociation. The J-V characteristics of the devices based

View Article Online
DOI: 10.1039/C6RA10442H

on the active layers processed with optimized DIO/CF are shown in Fig. 4a and 4c (red color) and corresponding photovoltaic parameters are summarized in Table 3. Comparing to the devices based on the active layer processed with CF, the devices processed with DIO (1v%)/CF showed higher PCE i.e. 4.06% (J_{sc} = 8.88 mA/cm^2, V_{oc} = 0.88 V, and FF = 0.52) and 5.31% (J_{sc}=11.16 mA/cm^2, V_{oc}=0.85 V, and FF= 0.56) for **DPP3** and **DPP4**, respectively. The enhancement in the PCE is attributed to the increase in both J_{sc} and FF. The enhancement in J_{sc} with DIO additive is consistent with the IPCE spectra as shown in Fig. 3b and 3d (red color), where the IPCE value has been increased throughout the entire wavelength region of measurement. The calculated J_{sc} values of devices from the IPCE spectra are 8.76 mA/cm^2 and 11.08 mA/cm^2, for **DPP3** and **DPP4** based devices respectively which are in good agreement with measured values.

The origin of increase in the J_{sc} for the devices processed with DIO/CF was investigated by absorption spectra of active layers. Fig. 5a and 6b show UV-visible optical absorption spectra of active layers processed with and without DIO additive. As compared to CF cast active layer, the DIO additive films showed a red shift, corresponding to the DPPs. This red shift is an indication of the improved ordered structure of active layer. Moreover, the absorption intensity, particularly the absorption band corresponds to DPP also increased. The broader absorption profile and increase in the absorption intensity, results more exciton generation in the active layer and may be one of the reasons for the increase in J_{sc}.

It is well known that the nanoscale morphology of BHJ active layer can be strongly affected by the solvent processing. [17] The X-ray diffraction pattern gives information about the molecular packing, crystallinity and D-A phase separation. [18] To get information about the effects of DIO additive on above parameter, XRD measurements were carried out on the pristine films of **DPP3**:$PC_{71}BM$ and **DPP4**:$PC_{71}BM$, spin cast from CF and DIO (1 v%)/CF and shown in Fig. 7a and 7b. The blend film cast from CF showed weak broad scatting at 2θ = 5.53° and 5.98°, for **DPP3** and **DPP4**, respectively, corresponding to the d-spacing of 1.34 nm and 1.18 nm, which is originated from very small crystalline domains of **DPP3** and **DPP4** respectively. [19] It can be seen that the diffraction peak for **DPP4** is stronger than that for **DPP3**, indicating more ordered stacking existed in **DPP4**, due to the additional TPA donor unit, consequential improved crystallinity, which is in agreement with the absorption spectra of **DPP4**. It was observed that with the addition of additive DIO in CF, the **DPP**s:$PC_{71}BM$ blended films shows the diffraction peaks with increased diffraction intensity, indicates that the processing additive significantly enhance the crystallinity of DPP in the active layer and

View Article Online
DOI: 10.1039/C6RA10442H

thus increase the degree of order. This can be interpreted that the processing additive allows the DPPs to crystallize more completely by providing increased drying time during the film formation. [20] Moreover, reduction in the d-spacing is related to the more closed packing, which is beneficial for efficient charge transport within the active layer. [21]

The transmission electron microscopy (TEM) of blended film of **DPP4** and $PC_{71}BM$ are shown in Fig. 8. The bright regions can be attributed to **DPP4** domains, whereas the dark regions can be attributed to $PC_{71}BM$ domains due to its high electron scattering density. [22] Without DIO additive, **DPP4**:$PC_{71}BM$ films showed large phase separation of the order of 35 – 40 nm, which indicates a limited interface between **DPP4** and $PC_{71}BM$. However, when 1% DIO was added, the blend film morphology for DIO/CF processed film slightly changed, revealing the small phase separation in the range of 25 – 30 nm, leading the increase in the interfacing area for exciton dissociation. Similar change in the morphology was observed in **DPP3**:$PC_{71}BM$ active layer. In general, the $PC_{71}BM$ component in the active layer is selectively soluble in less volatile solvent such as DIO, therefore, addition of DIO results aggregation of the donor material during the film drying process leading to formation of more highly ordered D – A phases, leading efficient charge transport. [23]

We further investigated the effect of solvent additive on the charge transporting properties of active layers, measuring the J-V characteristics of hole only devices employing the active layers processed with DIO (1v%/CF) (Fig. 5a and 5b red color) as described earlier. The hole mobilities are compiled in Table 3. The electron mobility of the solvent additive active layers is almost same as for CF cast active layer. It was observed that the blended films cast from CF exhibited very low hole mobilities and relatively high electron mobilities. The low hole mobilities and the unbalanced electron/hole transport are the main reasons for poor performance of the devices based on the active layers without solvent additives. Solvent additive significantly enhance the hole mobility to 4.26×10^{-5} and 9.18×10^{-5} cm^2/Vs for **DPP3** and **DPP4**, respectively. The addition of DIO, greatly increases the hole mobility for both blended films, indicates that the enhancement in the crystallinity induced by DIO can promote the vertical percolate pathways for blended films. In addition, the electron mobility significantly improved for the active layer processed with solvent additive, and more balanced electron/hole transport (5.68 and 2.71 for **DPP3** and **DPP4**, respectively) was achieved. The relative more balanced charge transport is in good agreement with increased FF of the devices.

The improved PCE of the devices with solvent additive processed active layers are supported by the relation of photocurrent density (J_{ph}) with effective voltage (V_{eff}). $J_{ph} = J_L$-

View Article Online
DOI: 10.1039/C6RA10442H

J_D, where J_L and J_D are the current densities under illumination and in dark, respectively. V_{eff} = V_o-V_{app}, V_o is the voltage at which J_{ph}= 0 and V_{app} is applied voltage [24]. The variation of J_{ph} with V_{eff} for the devices based on **DPP4**:$PC_{71}BM$ processed with CF and DIO (1v%)/CF are shown in Fig. 9. Similar plots have been observed for **DPP3**:$PC_{71}BM$ based devices. In the case of device based on active layer processed with CF solvent, J_{ph} shows stronger field dependence across the large bias range and has not fully saturate even V_{eff} = 3.0 V, suggesting a significant germinate and /or bimolecular recombination and less efficient charge collection at the electrodes, thus a lower FF. However, the device processed with DIO/CF, J_{ph} has a linearly dependence on voltage at the low value of V_{eff}, and J_{ph} reaches saturation, when the effective voltage reaches to 2.4 V and 2.0 V, for **DPP3**:$PC_{71}BM$ and **DPP4**:$PC_{71}BM$ active layer, respectively. This suggest that the photogenerated excitons are dissociated into free charge carriers and charge carriers are collected at the electrodes efficiently with reduced bimolecular recombination for the devices based on blends processed with DIO/CF. We have estimated the maximum generation rate of free charge carriers G_{max}, according to J_{phsat} = $qG_{max}L$, where q is the elementary charge and L is the active layer thickness. The G_{max} is influenced by the solvent additive with the values 0.96 $x10^{27}$ m^3s^{-1}, $2.1x10^{27}m^3s^{-1}$, 1.08 $x10^{27}$ m^3s^{-1} and 3.4 $x10^{27}m^3s^{-1}$ for **DPP3**:$PC_{71}BM$ (CF cast), **DPP3**:$PC_{71}BM$ (DIO/CF cast), **DPP4**:$PC_{71}BM$ (CF cast) and **DPP4**:$PC_{71}BM$ (DIOCF cast), respectively. The trend observed for G_{max} with different treatments is consistent with the enhancement of J_{sc} as well as the UV-visible absorption coefficient, indicating more efficient exciton generation and separation in the devices with DIO/CF cast. The ratio of J_{ph}/J_{sat} under short circuit conditions gives information about the overall exciton dissociation and charge collection efficiency. Under short circuit conditions, the ratios are 0.56, 0.72, 0.63 and 0.78 for **DPP3**:$PC_{71}BM$ (CF cast), **DPP3**:$PC_{71}BM$ (DIO/CF cast), **DPP4**:$PC_{71}BM$ (CF cast) and **DPP4**:$PC_{71}BM$ (DIO/CF cast), respectively. The greater value of P_C with DIO/CF processed devices is attributed to the better phase separation in the active layer, increased hole mobility, improved balance in charge transport and enhancement in the light absorption ability.

Conclusions

In conclusion, we have synthesized unsymmetrical and symmetrical triphenylamine based diketopyrrolopyrroles (**DPP3** and **DPP4**) by Sonogashira cross-coupling reaction and investigated their optical, thermal, electrochemical and computational properties. The red shift in the absorption spectra of **DPP4** compared to **DPP3** is related to extended conjugation and increased of donor-acceptor interaction. The HOMO and LUMO energy levels suggested

View Article Online
DOI: 10.1039/C6RA10442H

that these DPPs can be used as electron donor along with $PC_{71}BM$ as electron acceptor for the fabrication of solution processed small molecule bulk heterojunction solar cells. The solution processed BHJ small molecule processed with CF solution showed PCE of 2.23% and 3.05% for **DPP3**:$PC_{71}BM$ and **DPP4**:$PC_{71}BM$ active layers, respectively. The higher PCE of device based on the later active layer than that of former is attributed to the broader absorption profile of **DPP4** and larger hole mobility. In an attempt to improve the PCE, we have the adopted solvent additive (SA), i.e. 1% v DIO/CF technique and achieved PCE of 4.06% and 5.31%, for **DPP3**:$PC_{71}BM$ and **DPP4**:$PC_{71}BM$ active layer, respectively. The enhancement in the PCE with solvent additive based device is attributed to the balanced charge transport, higher light harvesting ability, and better nanoscale morphology for exciton dissociation and charge transport and collection, supported by the, XRD, TEM and mobility results. The results presented here shows that symmetrical **DPP4** shows higher PCE than unsymmetrical **DPP3** and employing additional ethyne bridged triphenylamine unit results in increased efficiency (PCE) of device from of 4.06% to 5.31%.

Supplementary data

Supporting information is available: Experimental, TGA curves, ^{1}NMR, ^{13}C NMR spectra and HRMS data of compounds.

Acknowledgments

Y. P. thanks Ministry of Human Resource Development (MHRD), R. M. thanks Department of Science and Technology (Project No. EMR/2014/001257) and the Council of Scientific and Industrial Research (Project No. 01/(2795)/14/emr-II), New Delhi for the financial support. GDS is thankful to DST, Government of India (DST-RFBR Joint Research Project). F.C. Chen thanks the support by the Ministry of Science and Technology of Taiwan (grant number: MOST 103–2923-E-009-001-MY3). We are also thankful to Faculty of Physics, Lomonosov Moscow State University, 1-2 Leninskiye Gory, Moscow, 119991, Russian Federation.

References

1. (a) S. Günes, H. Neugebauer and N. S. Sariciftci, *Chem. Rev*., 2007, **107**, 1324–1338; (b) R. Service, Solar energy Outlook brightens for plastic solar cells, *Science* (New York, NY) 2011, **332**, 293; (c) A. J. Heeger, *Adv. Mater*., 2014, **26**, 10-28; (d) Y. Huang, E. J. Kramer, A. J. Heeger and G. C. Bazan, *Chem. Rev.,* 2014, **114**,

View Article Online
DOI: 10.1039/C6RA10442H

7006−7043; (e) L. Dou, Y. Liu, Z. Hong, G. Li and Y. Yang, *Chem. Rev.,* 2015, **115** (23), 12633–12665; (f) L. Lu, T. Zheng, Q. Wu, A. M. Schneider, D. Zhao and L. Yu, *Chem. Rev.*, 2015, **115** (23), 12666–12731.

2. (a) Y. Liu, J. Zhao, Z. Li, C. Mu, W. Ma, H. Hu, K. Jiang, H. Lin, H. Ade and H. Yan, *Nat. Commun*., 2014, **5**, 5293; (b) Z. He, B. Xiao, F. Liu, H. Wu, Y. Yang, S. Xiao, C. Wang, T. P. Russell and Y . Cao, *Nat. Photonics,* 2015, **9**, 174; (c) Y. Yang, W. Chen, L. Dou, W. H. Chang, H. S. Duan, B. Bob, G. Li and Y. Yang, *Nat. Photonics,* 2015, **9**, 190; (d) J. D. Chen, C. Cui, Y. Q. Li, L. Zhou , Q.-D. Ou, C. Li, Y. Li and J.-X. Tang, *Adv. Mater.,* 2015, **27**, 1035–1041.
3. (a) H. Feng and Y. Luping, *J. Phys. Chem. Lett*., 2011, **2** (24), *3102*–3113; (b) O. P. Lee, A. T. Yiu, P. M. Beaujuge, C. H. Woo, T. W. Holcombe, J. E. Millstone, J. D. Douglas, M. S. Chen and J. M. J. Frechet, *Adv. Mater.,* 2011, **23**, 5359-5363; (c) B. Walker, A. B. Tamayo, X.-D. Dang, P. Zalar, J. H. Seo, A. Garcia, M. Tantiwiwat and T.-Q. Nguyen, *Adv. Funct. Mater*., 2009, **19**, 3063-3069.
4. (a) R. C. Coffin, J. Peet, J. Rogers and G. C. Bazan, *Nat. Chem*., 2009, **1**, 657-61; (b) Y. Z. Lin, Y. F. Li and X. W. Zhan, *Chem. Soc. Rev.,* 2012, **41**, 4245–4272; (c) M. P. Nikiforov, B. Lai, W. Chen, S. Chen, R. D. Schaller, J. Strzalka, J. Maser and S. B. Darling, *Energy Environ. Sci*., 2013, **6**, 1513 –1520.
5. (a) A. K. K. Kyaw, D. H. Wang, D. Wynands, J. Zhang, T. Q. Nguyen, G. C. Bazan and A. J. Heeger, *Nano Lett*., 2013, **13**, 3796-3801; (b) Y. Liu, C. C. Chen, Z. Hong, J. Gao, Y. Yang, H. Zhou, L. Dou and G. Li, *Sci. Rep.,* 2013, **3**, 3356.
6. (a) J. W. Lee, Y. S. Choi and W. H. Jo, *Org. Electron.,* 2012, **13**, 3060−3066; (b) S. Shen, P. Jiang, C. He, J. Zhang, P. Shen, Y. Zhang, Y. Yi, Z. Zhang, Z. Li and Y. Li, *Chem. Mater*., 2013, **25**, 2274−2281; (c) M. Cheng, C. Chen, X. Yang, J. Huang, F. Zhang, B.; Xu and Li. Sun, *Chem. Mater*., 2015, **27**, 1808−1814.
7. (a**)** Z. Hao and A. Iqbal, *Chem. Soc. Rev*., 1997, **26**, 203–213; (b) O**.** Wallquist, in *High-Performance Pigments*, ed. H. M. Smith, Wiley-VCH, Weinheim 2002, 159–184; (c) J. S. Zambounis, Z. Hao and A. Iqbal, *Nature,* 1997, **388**, 131–132.
8. (a) S. Qu and H. Tian, *Chem. Commun.*, 2012, **48**, 3039−3051; (b) J. Liu, Y. Sun, P. Moonsin, M. Kuik, C. M. Proctor, J. Lin, B. B. Hsu, V. Promarak, A. J. Heeger and T.-Q. Nguyen, *Adv. Mater*., 2013, **25**, 5898−5903; (c) Y. Lin, Y. Li and X. A. Zhan, *Adv. Energy. Mater*., 2013, **3**, 724−728; (d) V. S. Gevaerts, E. M. Herzig, M. Kirkus, K. H. Hendriks, M. M. Wienk, J. Perlich, P. Müller-Buschbaum and R. A. J. Janssen, *Chem. Mater*., 2014, **26**, 916−926; (e) L. Fu, W. Fu, P. Cheng, Z. Xie, C. Fan, M. Shi,

View Article Online
DOI: 10.1039/C6RA10442H

J. Ling, J. Hou, X. Zhan and H. Chen, *J. Mater. Chem. A,* 2014, **2**, 6589−6597; (f) W. Shin, T. Yasuda, Y. Hidaka, G. Watanabe, R. Arai, K. Nasu, T. Yamaguchi, W. Murakami, K. Makita and C. Adachi, *Adv. Energy Mater.,* 2014, **4**, 1400879-1400888; (g) Q.-R. Yin, J.-S. Miao, Z. Wu, Z.-F. Chang, J.-L. Wang, H.-B. Wu, Y. Cao and *J. Mater. Chem. A,* 2015, **3**, 11575−11586; (h) Y. Lin, L. Ma, Y. Li, Y. Liu, D. Zhu and X. Zhan, *Adv. Energy Mater*., 2013, **3**, 1166−1170.

9. (a) J.-L. Wang, Z. Wu, J.-S. Miao, K.-K. Liu, Z.-F. Chang, R.-B. Zhang, H.-B. Wu and Y. Cao, *Chem. Mater*., 2015, **27**, 4338−4348; (b) H. Qin, L. Li, F. Guo, S. Su, J. Peng, Y. Cao and X. Peng, *Energy Environ. Sci*., 2014, **7**, 1397–1401.
10. (a) J. W. Jung, F. Liu, T. P. Russell and W. H. Jo, *Energy Environ. Sci*., 2012, **5**, 6857–6861; (b) H. Choi, S.-J. Ko, T. Kim, P.-O. Morin, B. Walker, B. H. Lee, M. Leclerc, J. Y. Kim and A. J. Heeger, *Adv. Mater*., 2015, **27**, 3318–3324.
11. (a) Y. Patil, T. Jadhav, B. Dhokale and R. Misra, *Asian J. Org. Chem.,* 2016, DOI: 10.1002/ajoc.201600194; (b) Y. Patil, R. Misra, A. Sharma and G. D. Sharma, *Phys. Chem. Chem. Phys*., 2016, **18**, 16950-16957; (c) B. Dhokale, T. Jadhav, S. M. Mobin, and R. Misra, *RSC Adv.,* 2015, **5**, 57692–57699; (d) T. Jadhav, R. Maragani, R. Misra, V. Sreeramulu, D. N. Rao and S. M. Mobin, *Dalton Trans*., 2013, **42**, 4340–4342; (e) R. Misra, P. Gautam, T. Jadhav and S. M. Mobin, *J. Org. Chem.,* 2013, **78**, 4940–4948.
12. (a) T. Roland, E. Heyer, L. Liu, A.Ruff, S. Ludwigs, R. Ziessel, and S. Haacke, *J. Phys. Chem. C*, 2014, **118** (42), 24290–24301; (b) E. Heyer and R. Ziessel, *J. Org. Chem.*, 2015, **80** (13), 6737–6753.
13. M. Seri, A. Marrocchi, D. Bagnis, R. Ponce, A. Taticchi, T. J. Marks and A. Facchetti, *Adv. Mater*., 2011, **23**, 3827-3831.
14. C. H. Woo, P. M. Beaujuge, T. W. Holcombe, O. P. Lee and J. M. J. Frechet, *J. Am. Chem. Soc*., 2010, **132**, 15547–15549.
15. Y. Patil, T. Jadhav, B. Dhokale and R. Misra, *Eur. J. Org. Chem*., 2016, **4**, 733–738; (b) Y. Patil, R. Misra, M. L. Keshtov and G. D. Sharma, *J. Phys. Chem. C*, 2016, **120**, 6324−6335.
16. (a) Y. Sun, G. C. Welch, W. L. Leong, C. J. Takacs, G. C. Bazan and A. J. Heeger, *Nat. Mater*., 2012, **11**, 44–48; (b) J. K. Lee, W. L. Ma, C. J. Brabec, J. Yuen, J. S. Moon, J. Y. Kim, K. Lee, G. C. Bazan and A. J. Heeger, *J. Am. Chem. Soc*., 2008, **130**, 3619–3623.

View Article Online
DOI: 10.1039/C6RA10442H

17. Y. Huang, W. Wen, S. Mukherjee, H. Ade, E. J. Kramer and G. C. Bazan, *Adv. Mater*., 2014, **26**, 4168–4172.
18. (a) S.-S. Cheng, P.-Y. Huang, M. Ramesh, H.-C. Chang, L.-M. Chen, C.-M. Yeh, C.-L. Fung, M.-C. Wu, C.-C. Liu, C. Kim, H.-C. Lin, M.-C. Chen and C.-W. Chu, *Adv. Funct. Mater*., 2014, **24**, 2057–2063; (b) A. K. K. Kyaw, D. H. Wang, C. Luo, Y. Cao, T. Q. Nguyen, G. C. Bazan and A. J. Heeger, *Adv. Energy Mater*., 2014, **4**, 1301469.
19. (a) J. Huang, C. Zhan, X. Zhang, Y. Zhao, Z. Lu, H. Jia, B. Jiang, J. Ye, S. Zhang and A. Tang, *ACS Appl. Mater. Interfaces,* 2013, **5**, 2033–2039; (b) S. Zhang, B. Jiang, C. Zhan, J. Huang, X. Zhang, H. Jia, A. Tang, L. Chen and J. Yao, *Chem. Asian J.,* 2013, **8**, 2407 – 2416.
20. J. Peet, N. S. Cho, S. K. Lee and G. C. Bazan, *Macromolecules,* 2008, **41**, 8655–8659.
21. H. X. Zhou, L. Q. Yang and W. You, *Macromolecules,* 2012, **45**, 607–632.
22. X. N. Yang, J. Loos, S. C. Veenstra, W. J. H. Verhees, M. M. Wienk, J. M. Kroon, M. A. J. Michels and R. A. J. Janssen, *Nano Lett*., 2005, **5**, 579 –583.
23. (a) A. K. K. Kyaw, D. H. Wang, V. Gupta, W. L. Leong, L. Ke, G. C. Bazan and A. J. Heeger, *ACS Nano*., 2013, **7**, 4569–4577; (b) D. H. Wang, A. K. K. Kyaw, J.-R. Pouliot, M. Leclerc and A. J. Heeger, *Adv. Energy Mater*., 2014, **4**, 1300835; (c) B. Chen, Y. Yang, P. Cheng, X. Chen, X. Zhan and J. Qin, *J. Mater. Chem. A,* 2015, **3**, 6894- 6900.
24. (a) C. M. Proctor, M. Kuik and T. Q. Nguyen, *Prog. Polym. Sci*., 2013, **38**, 1941-1960; (b) P. W. M. Blom, V. D. Mihailetchi, L. J. A. Koster and D. E. Markov, *Adv. Mater.,* 2007, **19**, 1551–1566.

Table 1 Photophysical, electrochemical, thermal and computational properties of **DPP3** and **DPP4**.

	λ_{max} (nm) $\varepsilon/10^4$ ($M^{-1}.cm^{-1}$) [a]	λ_{max} (nm)[b]	$E_g^{opt}(eV)$ [c]	$E_g^{elect.}$ (eV)[d]	$E_g^{DFT}(eV)$[e]	T_e (°C)[f]
DPP3	583 (2.3), 551(2.8)	618	1.84	1.43	2.24	402
DPP4	627(3.3), 587(2.3)	658	1.72	1.30	2.07	398

[a]in dilute CF solution, [b]thin film cast from CF solution, [c] $E_g^{opt} = 1240/\lambda_{onset}$, λ_{onset} is onset absorption edge is absorption spectra in thin film, [d]estimated from electrochemical analysis,

View Article Online
DOI: 10.1039/C6RA10442H

[d]estimated from electrochemical analysis, [e]estimated from DFT calculation, [f]estimated from TGA.

Table 2 Electrochemical properties of **DPP3** and **DPP4**[a].

	E^2 Red	E^1 Red	E^1 Oxid	E^2 Oxid	E^3 Oxid	E^4 Oxid
DPP3	-1.51	-1.10	0.86	1.03	1.41	1.79
DPP4	-1.51	-0.89	0.91	1.22	1.47	1.82

[a]The electrochemical analysis was performed in a 0.1 M solution of Bu_4NPF_6 in dichloromethane at 100 mVs^{-1} scan rate, versus Ag/Ag^+ at 25 °C.

Table 3 Photovoltaic parameters for the BHJ organic solar cells using optimized **DPP3**:$PC_{71}BM$ and **DPP4**:$PC_{71}BM$ active layer under different processing conditions.

Active layer	J_{sc} (mA/cm^2)	V_{oc} (V)	FF	PCE (%)	μ_h (cm^2/Vs)	μ_e/μ_h
DPP3:$PC_{71}BM$[a]	6.74	0.92	0.36	2.23 (2.18)[c]	$5.34x10^{-6}$	44
DPP4:$PC_{71}BM$[a]	8.26	0.88	0.42	3.05 (2.98)[c]	$7.82x10^{-6}$	31
DPP3:$PC_{71}BM$[b]	8.88	0.88	0.52	4.06 (3.97)[c]	$4.26x10^{-5}$	5.68
DPP4:$PC_{71}BM$[b]	11.16	0.85	0.56	5.31(5.24)[c]	$9.18x10^{-5}$	2.71

[a]CF cast
[b]DIO/CF
[c]average to 8 devices

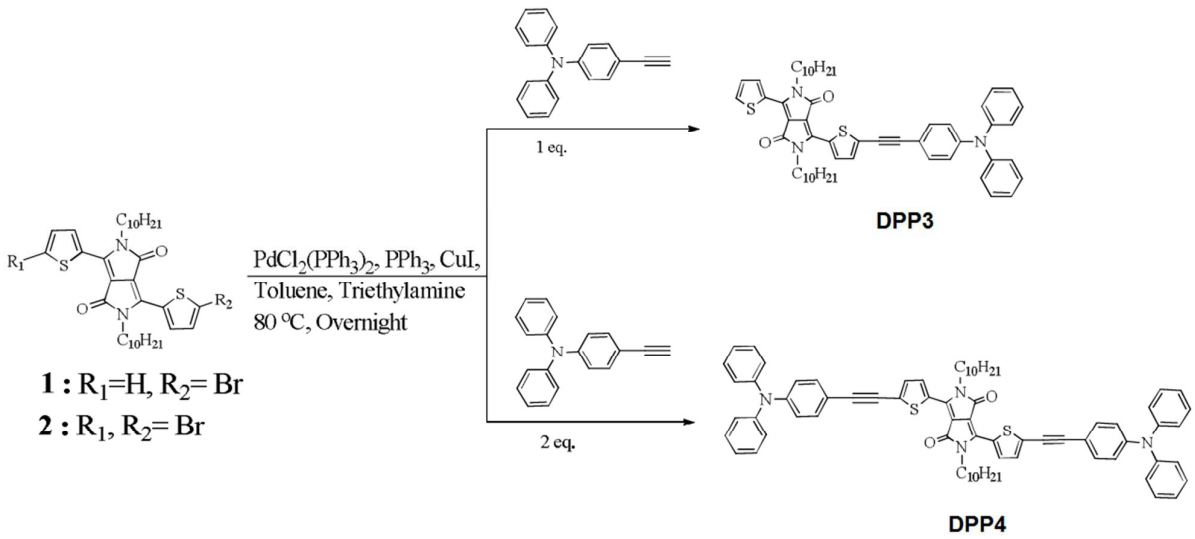

View Article Online
DOI: 10.1039/C6RA10442H

Scheme 1 Synthesis of triphenylamine based **DPP3** and **DPP4**.

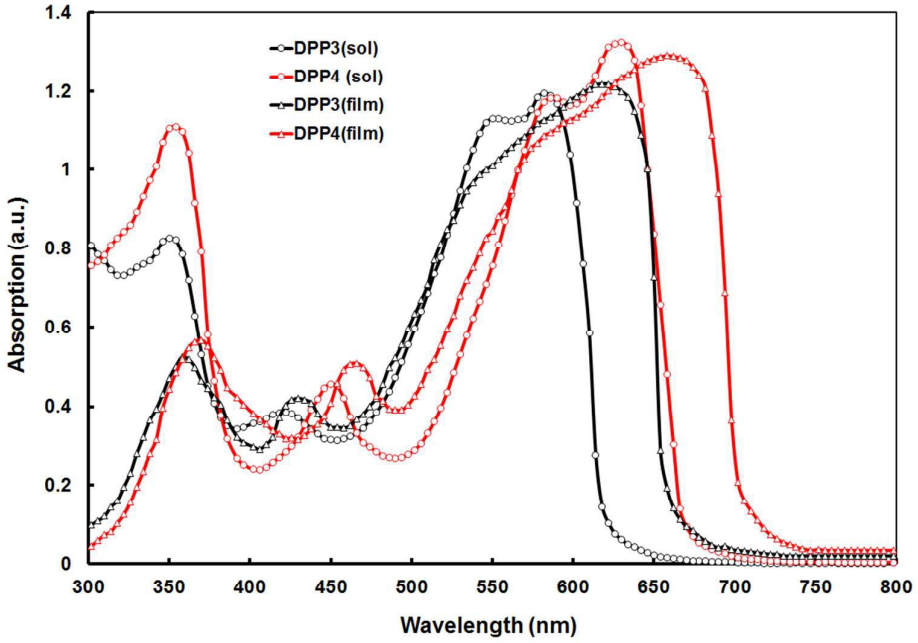

Fig. 1 Electronic absorption spectra of **DPP3** and **DPP4** in CF solution (10^{-4} M) and thin films cast from CF.

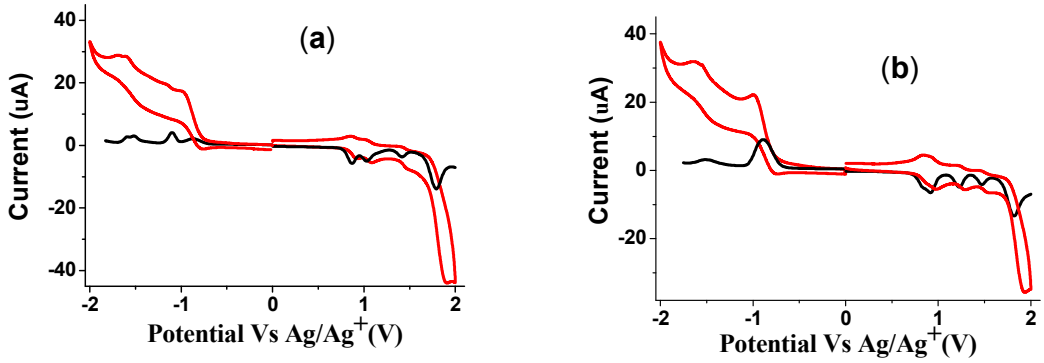

Fig. 2 cyclic voltammetry (CV) (red line) and differential pulse voltammetry (DPV) (black line) plots of (a) **DPP3** (b) and **DPP4.**

View Article Online
DOI: 10.1039/C6RA10442H

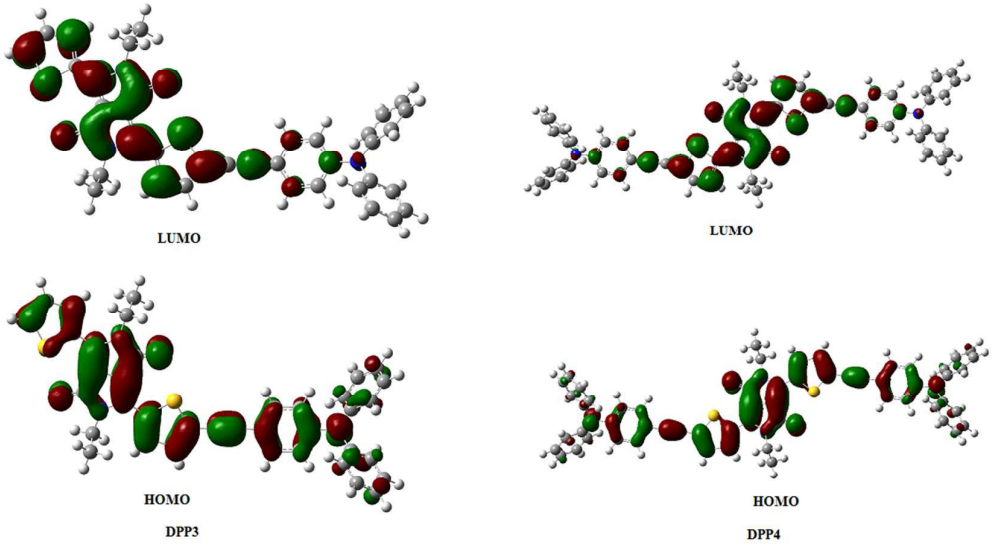

Fig. 3 The frontier molecular orbitals of **DPP3** and **DPP4** estimated by DFT calculations.

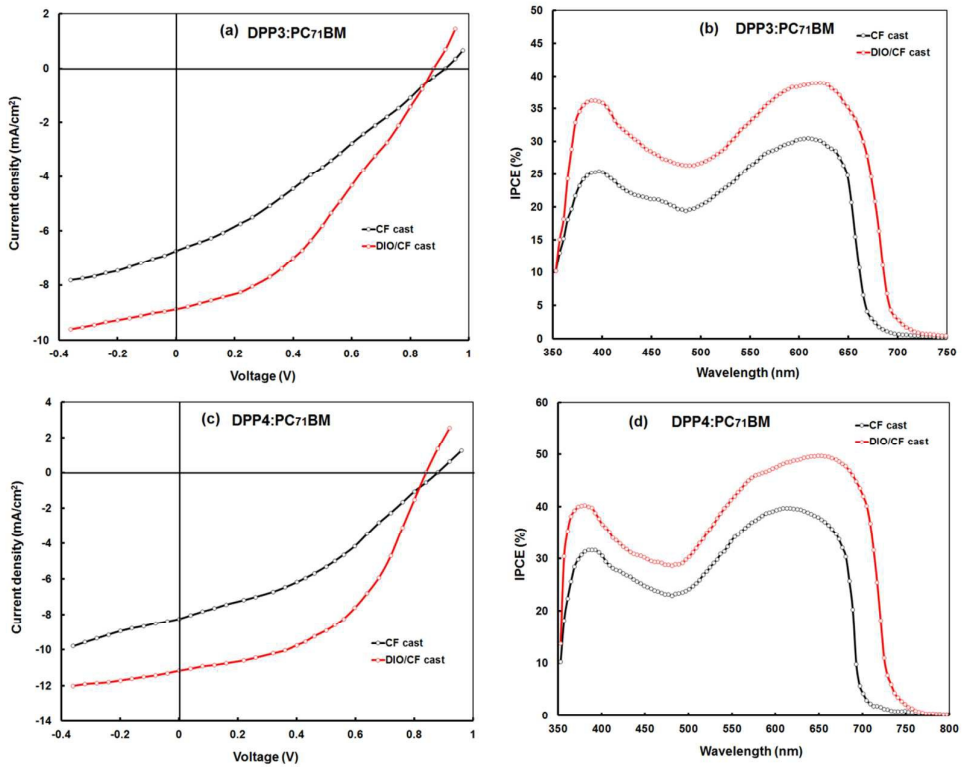

Fig. 4 Current –voltage (J-V) characteristics under illumination (AM15.G, 100 mW/cm^2) (a, c) and IPCE spectra (b, d) for the BHJ organic solar cells based on optimized **DPP3**:$PC_{71}BM$ and **DPP4**:$PC_{71}BM$ active layers cast from CF and DIO (3v%)/CF solutions.

View Article Online
DOI: 10.1039/C6RA10442H

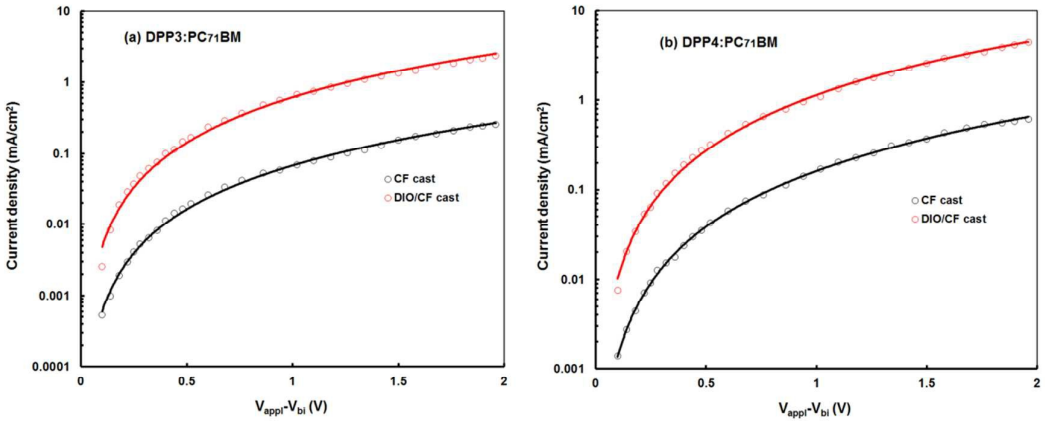

Fig. 5 Current –voltage (J-V) characteristics of the hole only devices based on (a) **DPP3**:$PC_{71}BM$ and (b) **DPP4**:$PC_{71}BM$ active layers processed with CF and DIO (3v%)/CF solutions. The solid lines represent the SCLC fitting.

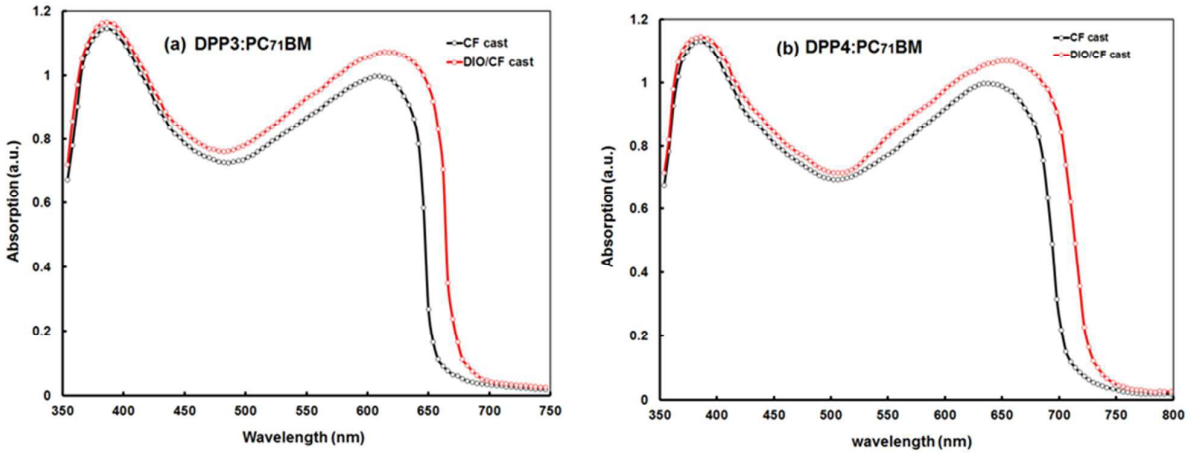

Fig. 6 Normalized absorption spectra of (a) **DPP3**:$PC_{71}BM$ and (b) **DPP4**:$PC_{71}BM$ thin films processed with and without DIO solvent additives.

View Article Online
DOI: 10.1039/C6RA10442H

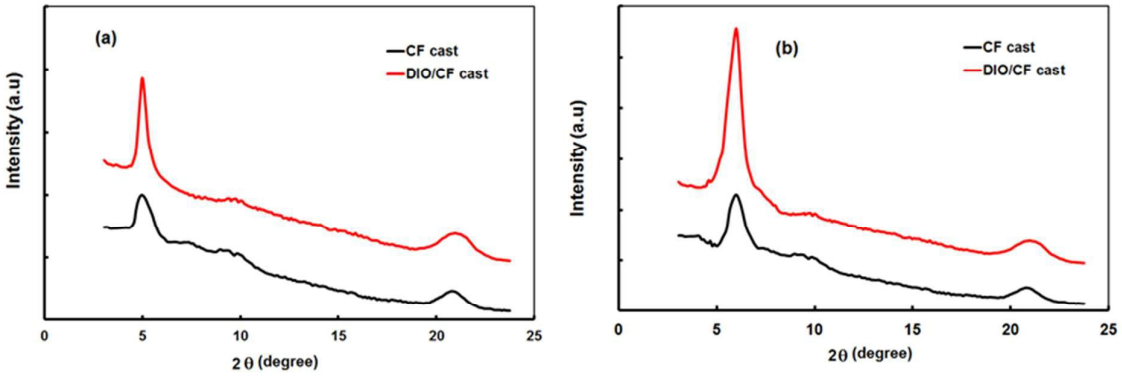

Fig. 7 XRD patterns of (a) **DPP3**:$PC_{71}BM$ and (b) **DPP4**:$PC_{71}BM$ thin films cast from CF and DIO/CF solutions.

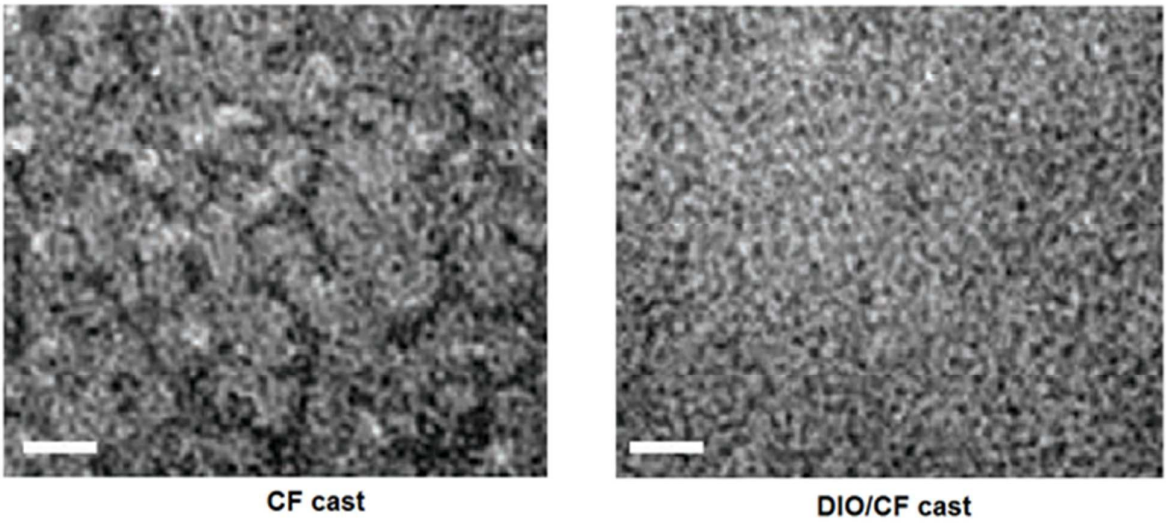

Fig. 8 TEM images of **DPP4**:$PC_{71}BM$ (1:2) films processed with CF and DIO/CF solution. The scale bar is 100 nm.

View Article Online
DOI: 10.1039/C6RA10442H

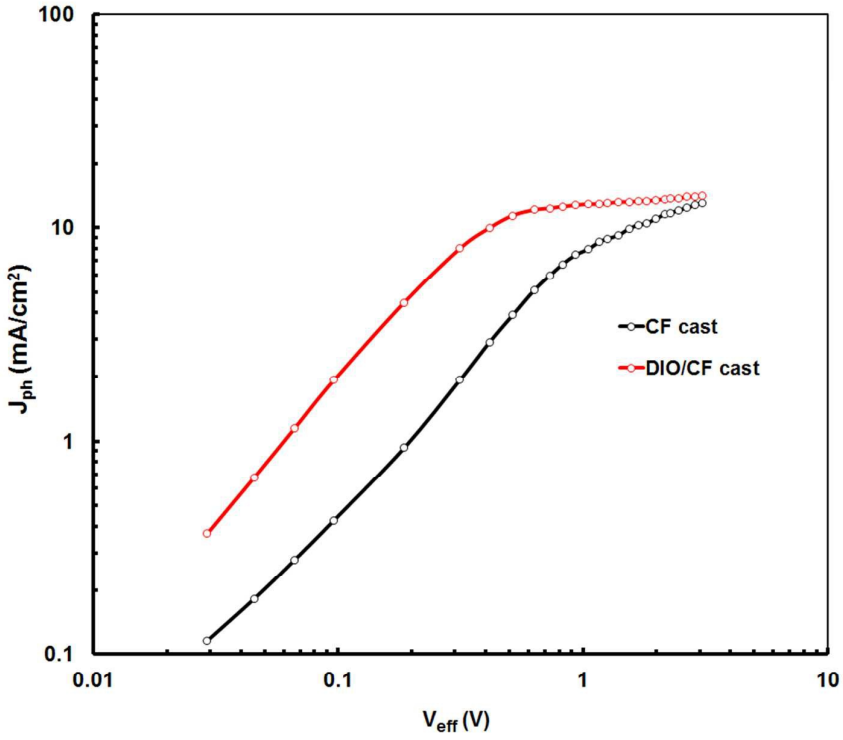

Fig. 9 Variation of Photocurrent density (J_{ph}) with effective voltage (V_{eff}) for devices based on **DPP4**:$PC_{71}BM$ processed with CF and DIO/CF solvents under constant incident light intensity.

TOC